ACSNANO

www.acsnano.org

ARTICLE

Full-Spectrum InP-Based Quantum Dots with Near-Unity Photoluminescence Quantum Efficiency

Hannes Van Avermaet, Pieter Schiettecatte, Sandra Hinz, Luca Giordano, Fabio Ferrari, Céline Nayral, Fabien Delpech, Janina Maultzsch, Holger Lange, and Zeger Hens*

Cite This: https://doi.org/10.1021/acsnano.2c03138

Read Online

ACCESS | Metrics & More | Article Recommendations | Supporting Information

ABSTRACT: Photoluminescent color conversion by quantum dots (QDs) makes possible the formation of spectrum-on-demand light sources by combining blue LEDs with the light generated by a specific blend of QDs. Such applications, however, require a near-unity photoluminescence quantum efficiency since self-absorption magnifies disproportionally the impact of photon losses on the overall conversion efficiency. Here, we present a synthesis protocol for forming InP-based QDs with +90% quantum efficiency across the full visible spectrum from blue/cyan to red. The central features of our approach are as follows: (1) the formation of InP core QDs through one-batch-one-size reactions based on aminophosphine as the phosphorus precursor, (2) the introduction of a core/shell/shell InP/Zn(Se,S)/ZnS structure, and (3) the use of specific interfacial treatments, most notably the saturation of the ZnSe surface with zinc acetate prior to ZnS shell growth. Moreover, we adapted the composition of the Zn(Se,S) inner shell to attain the intended emission color while minimizing line broadening induced by the InP/ZnS lattice mismatch. The protocol is established by analysis of the QD composition and structure using multiple techniques, including solid-state nuclear magnetic resonance spectroscopy and Raman spectroscopy, and verified for reproducibility by having different researchers execute the same protocol. The availability of full-spectrum, +90% QDs will strongly facilitate research into light−matter interaction in general and luminescent color conversion in particular through InP-based QDs.

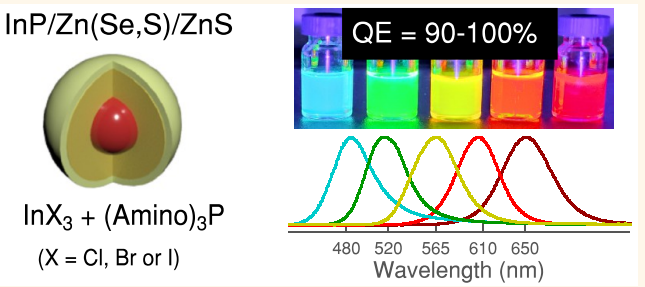

KEYWORDS: *optical materials, nanocrystals, core/shell, color conversion, monochromatic, restriction of hazardous substances*

Colloidal quantum dots (QDs) are outstanding luminescent materials. Their combining a spectrally narrow and tunable emission line with a suitability for solution-based processing spurred research into photoluminescent color conversion and electroluminescence for display, lighting and energy applications.[1−3] In particular, QDs based on CdSe, whose emission can cover the full color spectrum, were used to demonstrate display backlights with a bespoke red−green−blue emission spectrum,[4] high-color rendering white LEDs,[5] and luminescent solar concentrators[6] through the conversion of short-wavelength blue-to-UV light into saturated red and/or green light. In addition, full-spectrum CdSe QDs led to electroluminescent QD-LEDs emitting red, green, and blue light, by which full color displays were fabricated.[7] During the last 5 years, research on such technology demonstrators shifted to InP-based QDs, which are free of restricted elements such as cadmium or lead, and recent studies confirmed the potential of these QDs for optical downconversion and electroluminescence.[8,9]

A key characteristic of the photoluminescence of QDs is the fraction of absorbed photons that is re-emitted by a QD, i.e., the photoluminescence quantum yield (PLQY). Defined as an intrinsic, single-event absorption/emission property, PLQY provides an obvious upper limit to the external optical efficiency of luminescent color conversion by QDs. Even so, external device efficiencies can be significantly lower than the PLQY would suggest. Self-absorption of luminescent light by a QD ensemble can, for example, disproportionately magnify optical loss caused by a limited PLQY. Hence the widespread effort to develop colloidal QDs with a +90% PLQY, a figure at

Received: March 30, 2022
Accepted: June 13, 2022

https://doi.org/10.1021/acsnano.2c03138
ACS Nano XXXX, XXX, XXX−XXX

Table 1. Overview of InP-Based QDs with High PLQY Reported in the Literature and in This Study[a]

QDs	precursors: core shell	one-pot	PL peak (nm)	fwhm (nm)	QY (%)	ref
InP/ZnSe/ZnS	$InMy_3$, $(TMS)_3P$ $Zn(COOR)_2$, ODE-Se/S	no	535/618	35/42	90/93	13
InP/ZnSe/ZnS	$InLA_3$, $(TMS)_3P$, HF $ZnOA_2$, TOP-Se/S	no	630 528	35 36	98 95	8 12
Ga-InP/ZnSe/ZnS	InI_3, $ZnCl_2$, $(DMA)_3P$ GaI_3, $ZnSt_2$, TOP-Se/S	no	525	37	97	15
InP/ZnSe/ZnS	$InBr_3$, $ZnCl_2$, $(DMA)_3P$ $Zn(Pa)_2$, TOP-Se/S	no	621	44	86	17
InP/ZnSeS/ZnS	$InCl_3$, $ZnCl_2$, $(DMA)_3P$ $ZnSt_2$, TOP-Se/S	yes	614	63	80	16
InP/ZnSeS/ZnS	InI_3, $ZnBr_2$, $(DMA)_3P$ $ZnSt_2$, TOP-Se/S	yes	510	45	95	14
InP/ZnSe/ZnS	$InCl_3$, $ZnCl_2$, NaOCP $ZnSt_2$, TOP-Se/S	yes	533/620	36/52	97/95	18
InP/Zn(Se,S)/ZnS	InX_3, ZnX_2, $(DEA)_3P$ $ZnOA_2$, $ZnAc_2$, TOP-Se/S	yes	480−630	45	>90	This work

[a]The different columns give an outline of the QDs synthesized, the precursors used for core and shell synthesis, the use of a one-pot approach, and the emission characteristics including (PL peak) central wavelength, (fwhm) full width at half maximum of the emission line and PLQY. La, My, Pa, and St indicate laurate, myristate, palmitate, and stearate, respectively, while $(DMA)_3P$ and $(DEA)_3P$ refer to *tris*-dimethylaminophosphine and *tris*-diethylaminophosphine.

which the impact of successive reabsorption steps on the external quantum efficiency diminishes markedly (Supporting Information section S1).

Following the insight that the epitaxial overgrowth of an emissive core QD with a wide band gap semiconductor shell can considerably increase the PLQY,[10] near-unity PLQY was attained with CdSe/CdS structures emitting at around 600 nm.[11] As outlined in Table 1, similar results were recently obtained by the successive growth of ZnSe and ZnS shells around InP core QDs. For example, using InP QDs synthesized using tritrimethylsilylphosphine ($(TMS)_3P$), a 95% PLQY was obtained for green-emitting InP/ZnSe/ZnS QDs,[12] an intermediate HF etch of the InP surface led to 100% efficient, red-emitting InP/ZnSe/ZnS structures,[8] and similar results were obtained by implementing a purification step prior to shell growth.[13] Furthermore, equally efficient green emission was obtained with InP core QDs formed using amino-phosphines, either by means of a Zn(Se,S) shell growth,[14] or through the formation of an intermediate GaP layer,[15] while the best reported PLQYs of red-emitting InP-based QDs fall in the range of 80−86%.[16,17] In addition, near-unity PLQYs were recently reported for green and red emitting InP-based QDs synthesized from sodium phosphaethynolate.[18] Still, while showing the feasibility to attain +90% PLQY, few studies present a common strategy implemented within a single synthesis protocol to obtain such results across the full color spectrum from cyan/blue to red, neither in the case of CdSe- nor InP-based QDs.

Here, we report on a synthesis method for InP-based QDs that yields +90% PLQY across the full emission spectrum through straightforward rational adaptations of a common synthesis protocol executed within a one-pot reaction mixture. Focusing first on red-emitting InP-based QDs, we show that a succession of interfacial treatments and separate ZnSe and ZnS shell growth results in +90% PLQY emissive InP/ZnSe/ZnS QDs. Here, the intermediate ZnSe shell is essential to avoid broadening of the emission line by strain-induced sample heterogeneity. When reducing the InP core QD dimensions, a gradual admixing of sulfur to form an alloyed Zn(Se,S) intermediate shell helps to confine the electron−hole pair within the InP core and keep strain-induced line broadening to a minimum. Through this approach, we can seamlessly shift the emission line from red to cyan/blue while preserving +90% PLQY and keeping the line width below 50 nm. Having available such full-spectrum InP-based quantum dots with +90% PLQY will strongly promote the development of QD-based light sources with predesigned emission spectra optimized for high color rendering, display applications, or human centric lighting.

RESULTS AND DISCUSSION

Red-Emitting InP/ZnSe/ZnS Quantum Dots with Near-Unity Quantum Yield. We formed InP core QDs by reacting $InCl_3$ and diethylaminophosphine ($(DEA)_3P$) in oleylamine in the presence of $ZnCl_2$ using an established protocol,[19] and grew ZnSe shells by the subsequent addition of zinc oleate and trioctylphosphine selenium to the reaction mixture. Full details on this procedure are given in the "Methods" section and Supporting Information section S2. In the first instance, we used this approach to synthesize InP/ZnSe QDs emitting at 610 nm after ZnSe shell growth and evaluate the impact of different interfacial treatments in between the InP core formation and the ZnSe shell growth. In view of recent studies reporting a dependence between the InP core composition and the InP/ZnSe band-alignment or emission efficiency,[20,21] and between phosphate (PO_4^{3-}) at the core/shell interface and an enhanced PLQY,[22,23] we either injected (1) tetra-butylammonium hexafluorophosphate (TBA HFP), (2) water, or (3) a mixture of both in order to achieve better control over the composition of the core/shell interface. As outlined in Supporting Information section S3, these different treatments give rise to a considerable increase of oxidized phosphorus, ranging from 19% to 50 and 75%, as compared to the 6% of oxidized phosphorus found in a reference synthesis without interfacial treatment, while the addition of TBA HFP gives rise to some fluorination of the InP QD surface, mostly as partially fluorinated phosphorus.

https://doi.org/10.1021/acsnano.2c03138
ACS Nano XXXX, XXX, XXX−XXX

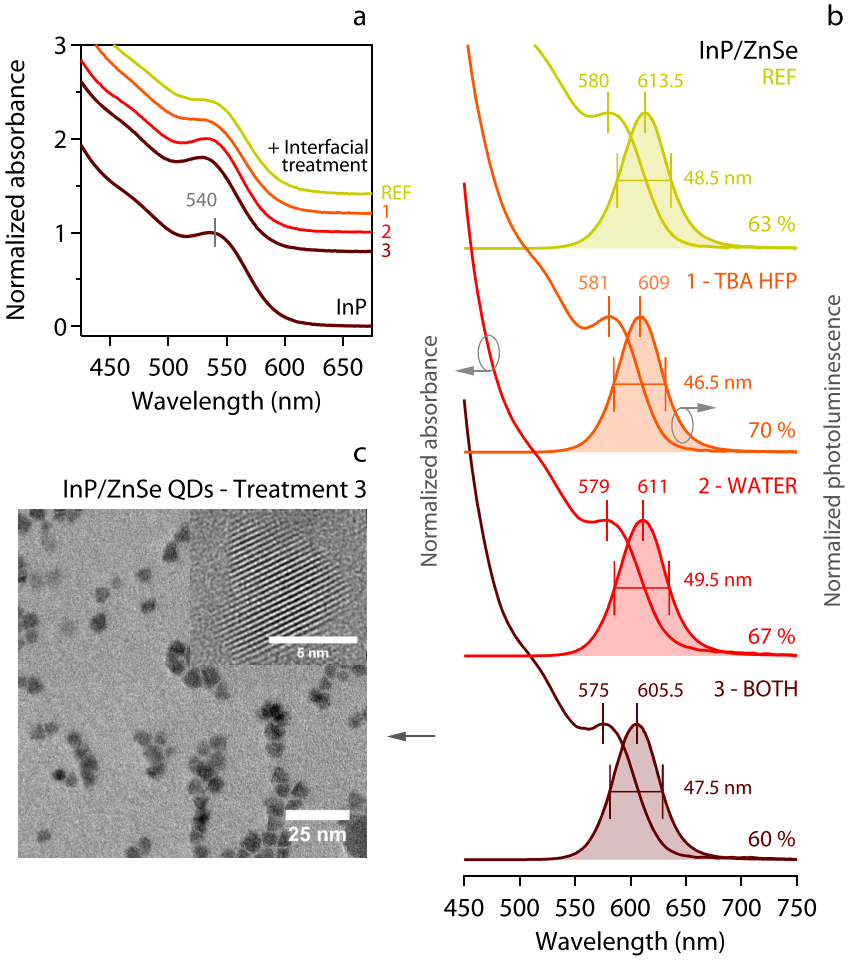

Figure 1. (a) Absorbance spectra of InP core QDs before and after an interfacial treatment involving (1) tetrabutyl ammonium hexafluorophosphate, (2) water, (3) both, or (REF) no treatment. The absorption band-edge feature is better defined after treatment consisting of water. Spectra have are offset for clarity. (b) Optical properties of InP/ZnSe QDs only differ slightly upon varying the interfacial treatment of InP core QDs. (c) TEM and HRTEM image of InP/ZnSe QDs produced with the double treatment.

As shown in Figure 1a, the comparison of different interfacial treatments was carried out using initial InP core QDs with highly similar characteristics, a point highlighting the reproducibility of InP QD formation via the aminophosphine route.[19,24] While we found that treatments 2 and 3, which involve water, better preserve the original band-edge feature in the absorbance spectrum, we observed little difference between the different treatments or the reference synthesis after shell growth. All emission spectra were centered around 610 nm, and the full-width at half-maximum (fwhm) of the emission line varied only slightly between treatment 1 (46.5 nm) and treatment 2 (49.5 nm; see Figure 1b). In addition, transmission electron microscopy (TEM) micrographs showed no significant alterations in size nor shape for the resulting InP/ZnSe QDs, see Figure 1c and Supporting Information section S3. Moreover, the addition of a ZnSe shell led to a similar increase of the PLQY of the band-edge emission, reaching 60−70% for all samples. Hence, opposite from the idea that suppression of surface oxidation is critical to obtain high-quality InP-based QDs,[8] we confirm previous findings that the photoluminescence efficiency of InP/ZnSe QDs can benefit from interfacial oxidation.[22] Still, an intriguing observation is the similarity between the different interfacial treatments and the reference, which only yielded 6% of oxidized phosphorus. Since surface oxidation of InP QDs by carboxylic acids is a known phenomenon,[25] we conjecture that the use of a zinc carboxylate, as opposed to zinc chloride,[22] to grow ZnSe shells suffices to create the interfacial oxide that is needed to passivate interfacial trap states. Our main conclusion of this analysis was that merely increasing or precisely controlling the amount of interfacial oxide appears, by itself, insufficient to attain the highest PLQY.

Recent studies highlighted that the shelling of InP/ZnSe QDs by addition of a ZnS layer can result in red and green InP/ZnSe/ZnS QDs with a near-unity PLQY,[8,12,15] starting from InP core QDs formed using tris(trimethylsilyl)phosphine and etched using HF prior to shell growth. We therefore extended our study to the formation of such a ZnS shell to further passivate aminophosphine-based InP/ZnSe QDs in a one-pot approach. Here, we continued first with InP/ZnSe core/shell QDs emitting at 610 nm formed using interfacial treatment 3, although we will show later that the possibility of attaining +90% PLQY is independent of the specific interfacial treatment implemented. In addition, we included an intermediate reaction step after the formation of InP/ZnSe but before ZnS shell growth that involved the addition of 5 equiv of zinc acetate, relative to the initial amount of $InCl_3$, to the reaction mixture. While long-chain zinc carboxylates are widely used to form ZnSe or ZnS shells around InP QDs,[8,12,15,16,26−29] few studies describe the use of zinc acetate

https://doi.org/10.1021/acsnano.2c03138
ACS Nano XXXX, XXX, XXX−XXX

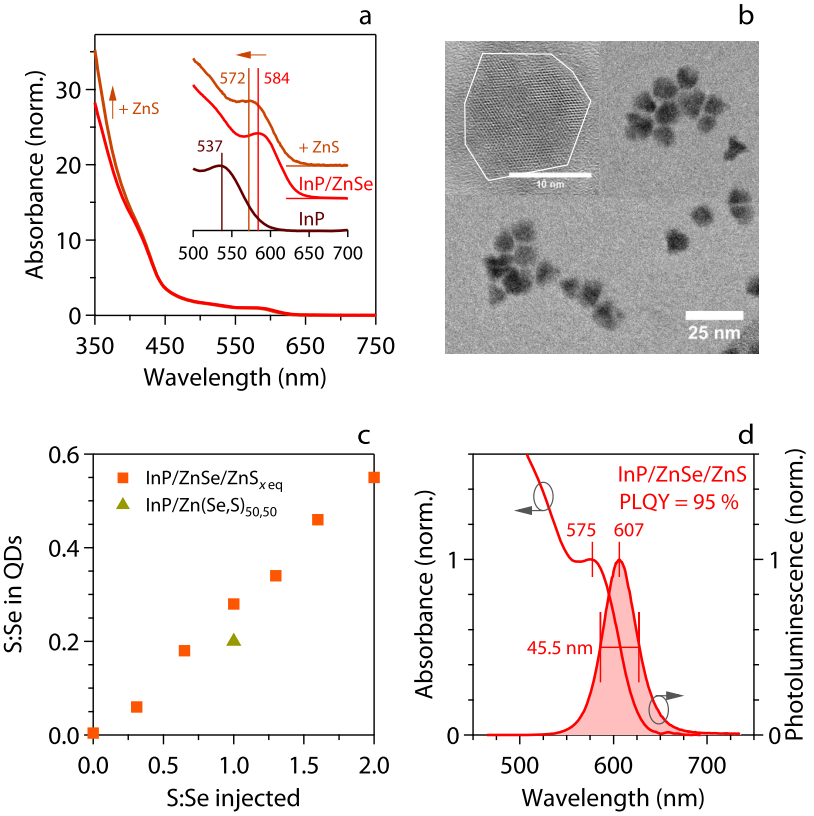

Figure 2. (a) Absorbance spectra at different stages of a synthesis of red-emitting InP/ZnSe/ZnS QDs. (b) TEM and HRTEM images of InP/ZnSe/ZnS QDs show a regular QD shape. The scale bar represents 10 and 25 nm, respectively, for the HRTEM and TEM images. (c) Energy-dispersive X-ray spectroscopy as elemental analysis tool demonstrates a linear correlation between the injected and incorporated sulfur in the InP/ZnSe/ZnS QDs. (d) Absorbance and emission spectra of InP/ZnSe/ZnS QDs. Spectra have been normalized relative to the maximum of the band-edge absorbance or emission.

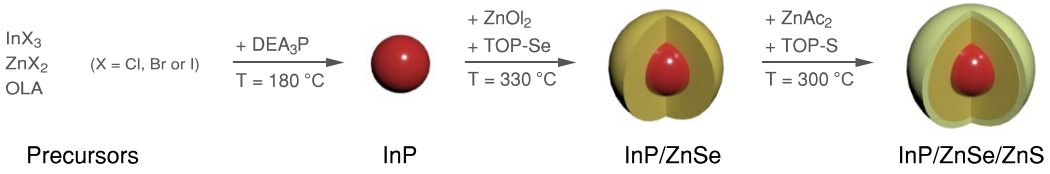

Figure 3. Synthesis scheme for InP/ZnSe/ZnS QDs using indium and zinc halides, tris(diethylamino)phosphine, zinc carboxylates, and tri-*n*-octylphosine selenide and sulfide in oleylamine and 1-octadecene.

in QD synthesis..[30,31] Still, we noted a pronounced brilliance in the reaction mixture after zinc acetate addition, which indicated a significant increase of the photoluminescence efficiency; see Supporting Information section S4. Possibly, the small zinc acetate molecule can more easily bind to undercoordinated selenium at the ZnSe outer surface, thereby eliminating nonradiative recombination centers more effectively than long-chain zinc carboxylates.

Following this intermediate zinc acetate addition, we injected trioctylphosphine sulfur (TOP-S) to form ZnS with unreacted zinc oleate and acetate already present in the reaction mixture. As indicated in Figure 2a, TOP-S addition induces a small blueshift of the band-edge absorption feature and additional absorbance at wavelengths shorter than ~350 nm, two changes indicative for a successful ZnS shell growth. We confirmed this conclusion by TEM imaging, which gave evidence of an average QD diameter of 10.8 nm, which is 1.4 nm larger than the initial InP/ZnSe core/shell QDs. Moreover, elemental analysis by energy-dispersive X-ray spectroscopy revealed that the resulting QDs contained sulfur in proportion to the amount of TOP-S added, see Figure 2b,c. Most interestingly, however, is the photoluminescence of the resulting InP/ZnSe/ZnS QDs. As shown in Figure 2d, we obtained a band-edge emission that is centered at 607 nm with a fwhm of 45.5 nm and PLQY of 95% as measured using an integrating sphere and excitation wavelength at 405 nm for the best sample. Moreover, repetitive execution of the same protocol by three different researchers led to batches with an average PLQY of 93%; see Supporting Information section S5. As can be seen in Table 1, such a PLQY is the highest reported for red-emitting, InP-based QDs formed using amino-phosphine as the phosphorus precursor.

Optimized InP/ZnSe/ZnS Quantum Dots through Strain Analysis. As outlined in Figure 3, the scheme we developed to form InP/ZnSe/ZnS core/shell QDs involves a sequence of crystal growth and interfacial treatment steps within a single, one-pot reaction mixture. Such a sequence leaves ample room for optimization, for example, by adjusting

https://doi.org/10.1021/acsnano.2c03138
ACS Nano XXXX, XXX, XXX−XXX

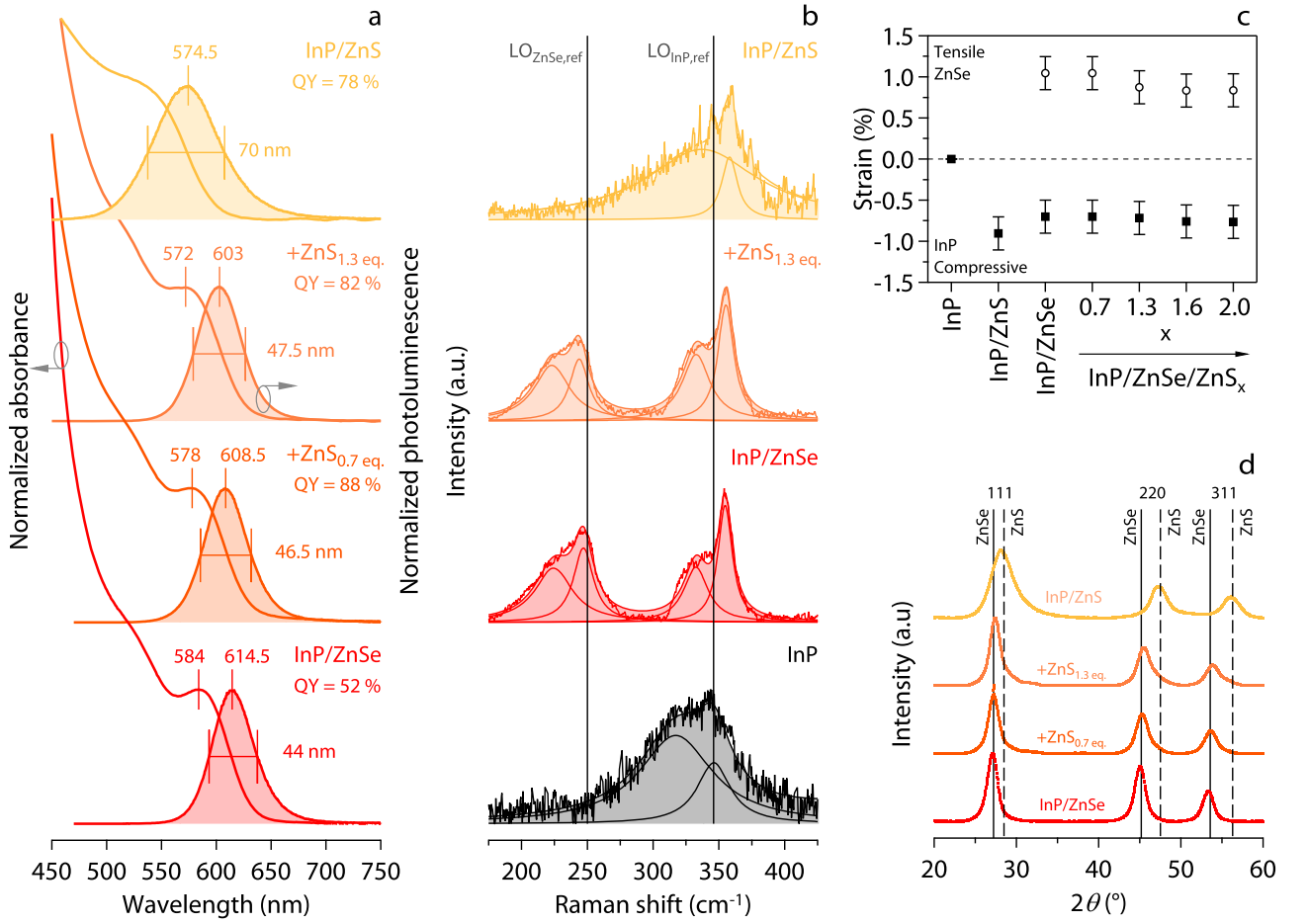

Figure 4. (a) Overview of absorption and emission spectra of series 1 samples, including (bottom-to-top) InP/ZnSe and InP/ZnSe/ZnS made using 0.7 and 1.3 equiv of TOP-S and InP/ZnS. All spectra have been normalized with respect to the absorbance or emission maximum at the band-edge transition as indicated. (b) Overview of Raman spectra of a series 1 sample, together with the InP core, the InP/ZnSe, and the InP/ZnS core/shell reference materials. The vertical lines indicate the reference wavenumber for the InP and ZnSe LO phonons used to calculated strain from the shift of the respective phonon lines. (c) Strain in the InP core (filled markers) and the ZnSe shell (open markers) for different series 1 samples, and the InP core and InP/ZnS core/shell reference samples. (d) X-ray diffraction patterns of series 1 samples as indicated. The vertical lines indicate the diffraction angles expected for zinc blende ZnSe and ZnS as indicated.

the amount of ZnSe and ZnS formed to maximize the PLQY and minimize the emission line width. While such an optimization could be approached through a design of experiments, we sought to relate for this study the strain within the InP/ZnSe core/shell QD structure to the amounts of ZnSe and ZnS used in the synthesis protocol. This approach was inspired by several reports indicating that optimal photoluminescence is obtained when strain in a core/shell structure is minimized[32−35] and the idea that a smaller lattice parameter mismatch with a substrate makes for more homogeneous shell growth. We therefore analyzed strain through Raman spectroscopy on two series of samples. A first (series 1) involves a single InP/ZnSe core/shell structure, overgrown by varying amounts of ZnS. In a second (series 2), we used aliquots of a single InP/ZnSe/ZnS structure synthesized at different stages of ZnSe and ZnS shell growth. Finally, also using an InP core, InP/ZnS, InP/ZnSe, and InP/$Zn(Se,S)_{50:50}$ core/shell QDs, made using the same InP core QDs as all other QDs analyzed, were included as benchmark materials. A full overview of the analysis on the benchmark QDs and the series 1 and 2 QDs is given in the Supporting Information sections S6−S8, respectively.

Figure 4a represent absorbance and photoluminescence spectra for series 1 samples, together with benchmark data recorded on InP/ZnS and InP/ZnSe core/shell QDs. Here, InP/ZnSe/ZnS QD samples are characterized by the equivalence of TOP-S used in the synthesis, relative to TOP-Se. As indicated in Figure 2c, the final sulfur/selenium ratio in the QDs is proportional to the TOP-S equivalence. Focusing on the photoluminescence, one sees that for the ZnSe shell thickness used for this experiment, overgrowth with ZnS results in a considerable increase of the PLQY, together with a small blueshift and a minor broadening of the band-edge emission. As outlined in Supporting Information section S7, the 44 nm wide emission band centered around 614.5 nm for InP/ZnSe widens to 49 nm and shifts to 604 nm when 2 equiv of TOP-S are used. This limited impact of ZnS overgrowth contrasts starkly with the considerable line broadening to 70 nm and the blueshift by almost 40 nm observed when ZnS is grown directly on similar InP core QDs.

Selected Raman spectra as recorded on series 1 InP/ZnSe/ZnS QDs, InP core, and InP/ZnS and InP/ZnSe core/shell QDs are depicted in Figure 4b. In agreement with previous studies,[34−36] the InP/ZnSe Raman spectrum exhibits two optical phonon bands at around 225−250 cm^{-1} and 335−360

https://doi.org/10.1021/acsnano.2c03138
ACS Nano XXXX, XXX, XXX−XXX

cm^{-1}. The band between 225 and 250 cm^{-1} can be attributed to the longitudinal optical phonon of ZnSe and an interface-related shoulder.[36] The band around 335−360 cm^{-1} can be assigned to transversal (TO) and longitudinal (LO) optical phonons of InP. Also here, one sees that ZnS shell growth around the InP/ZnSe core/shell QDs mostly preserves the Raman features of the InP core and the ZnSe shell (albeit with minor shifts reflecting strain), while direct ZnS shelling of InP core QDs results in a considerable broadening of the InP LO phonon line. For a quantitative analysis, we described the Raman spectra as a sum of Lorentzian fit functions (examples are included in Figure 4b) and used the resulting shifts $\frac{\Delta\omega}{\omega}$ of the InP and ZnSe LO phonon as compared to the InP and ZnSe reference, to estimate relative lattice constant changes $\frac{\Delta a}{a}$ according to refs 34 and 35:

$$\frac{\Delta\omega}{\omega} = \left(1 + 3\frac{\Delta a}{a}\right)^{-\gamma} - 1 \quad (1)$$

Here, $\gamma = -\frac{\partial \ln \omega}{\partial \ln V}$ with V being the unit cell volume, is the Grüneisen parameter, which we took as 1.24 and 0.85 for InP and ZnSe, respectively.[37−40] Following this analysis, Figure 4c indicates that ZnSe shelling results in a combination of compressive strain in the InP core and tensile strain in the ZnSe shell. In line with previous work,[34] the relatively small 3.4% lattice parameter mismatch between InP and ZnSe limits strain to ca. −0.75% in the InP core and ∼1% in the ZnSe shell. Further ZnS overgrowth slightly reduces the tensile strain in the ZnSe shell, as expected given the smaller lattice parameter of ZnS.

On the basis of the decomposition of the Raman spectrum, we estimated that direct growth of ZnS around InP core QDs results in a 1% compressive strain on the InP core. Being slightly larger than the strain brought about by ZnSe overgrowth, this result agrees with the larger lattice mismatch between InP and ZnS. However, this number probably underestimates the impact of direct growth of ZnS on the structure of the resulting InP/ZnS QDs. The widening of the band-edge emission and the pronounced broadening of the InP phonon line both point toward a considerable structural disorder, either within single QDs or between different QDs. This point is confirmed by the X-ray diffraction patterns of selected series 1 InP/ZnSe/ZnS samples shown in Figure 4d. While ZnS shell growth around InP/ZnSe core/shell QDs only leads to a slight shift of the diffraction features to larger angles and a minor peak broadening, direct growth of a ZnS shell on InP core QDs strongly broadens the diffraction features centered at the expected angles for ZnS. We thus conclude that the intermediate ZnSe shell is essential to mitigate the strong impact of the lattice mismatch between InP and ZnS on the QD structure and attain the narrowest emission lines.

Given this central role of the ZnSe intermediate shell, we continued this study by monitoring the evolution of the optical characteristics and the strain in core and shell as a function of the ZnSe shell thickness (series 2), for which we doubled the amount of TOP-Se as compared to the reference synthesis discussed in the previous section and used 0.4 equiv of TOP-S. Figure 5 summarizes the analysis of these series 2 reaction aliquots. A full overview is given in Supporting Information section S8. As can be seen, the formation of a ZnSe shell induces a redshift of the band-edge absorption from 550 nm to, eventually, 580 nm for the thickest ZnSe shells. This evolution

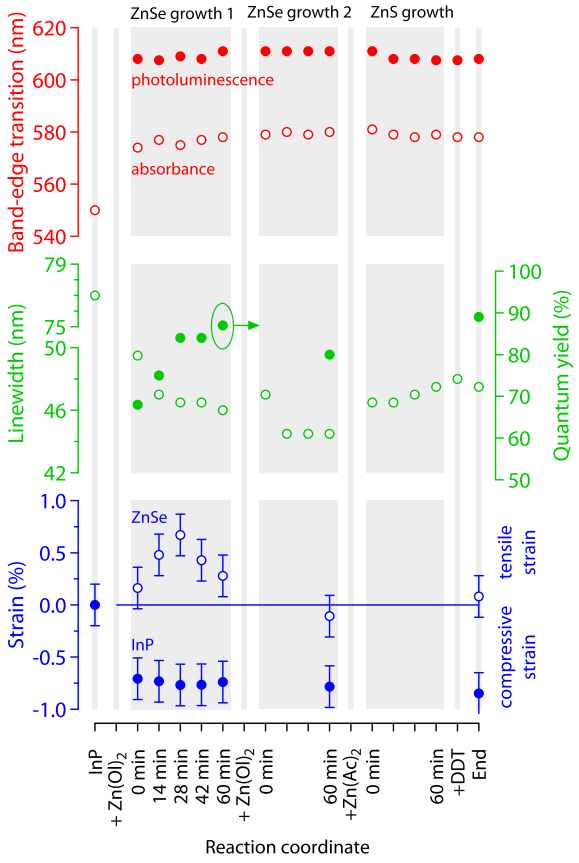

Figure 5. Variation of (red) central wavelength of the band-edge emission in (open markers) absorbance and (filled markers) photoluminescence spectra, (green filled markers) PLQY and (open markers) emission line width, and (blue) strain in (open markers) ZnSe and (filled markers) InP throughout a full synthesis sequence involving two ZnSe and one ZnS growth stage separated by interfacial treatments as indicated. Prior to purification of the final product, 1-dodecanthiol (DDT), was added to the reaction mixture.

is well-known from literature and is typically assigned to charge-carrier delocalization in the ZnSe shell. In addition, the progressive overgrowth of ZnSe induces a continuous reduction of the emission line width, which reaches 44.5 nm for the thickest ZnSe shells. However, the initial increase of the PLQY upon ZnSe shell growth, from 68 to 87% in this experiment, is reversed when shell growth continues; an evolution that may reflect the increasing difficulty to fully passivate larger ZnSe surfaces during synthesis or after purification. Interestingly, while ZnSe shell growth immediately results in compressive strain in the InP core, it appears that the ZnSe shell first experiences increasing tensile strain that is, however, completely relieved for the thickest ZnSe shells. In line with previous results of strain analysis for InP/ZnSe QDs,[41] this observation possibly indicates that ZnSe is initially deposited as partial shell islands that only merge into a complete, coherent ZnSe shell in the later stages of the reaction. This limiting situation concurs with the most narrow emission line, which could thus reflect the elimination of heterogeneity due to variations of the spectral redshift or core/shell strain across the QD ensemble related to slight differences in shell thickness. Finally, the addition of ZnS preceded by the zinc acetate interfacial treatment brings the PLQY to 90%, without further straining the InP core or the ZnSe shell. These

https://doi.org/10.1021/acsnano.2c03138
ACS Nano XXXX, XXX, XXX−XXX

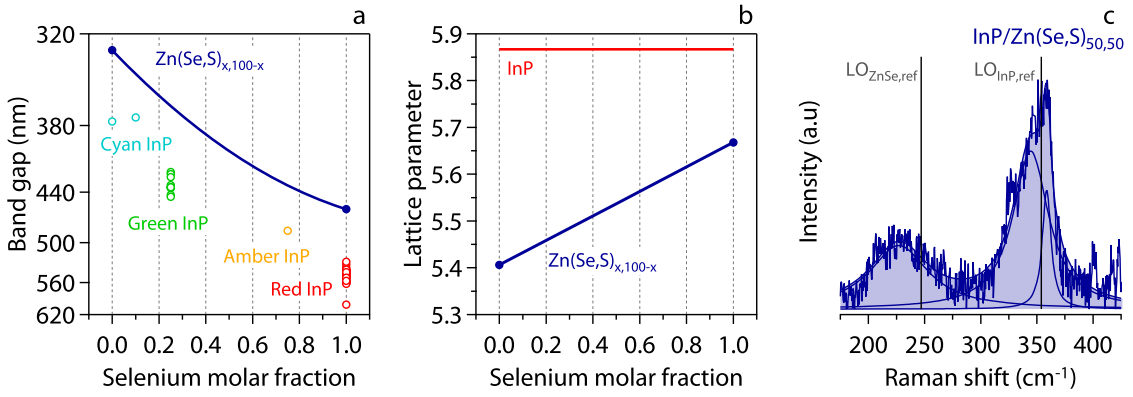

Figure 6. (a) Position of the band gap of the InP core QDs used to form red-, amber-, green-, and cyan-emitting core/shell QDs, relative to the bulk band gap of $Zn(Se,S)_{x,100-x}$, where x indicates the fraction of selenium. (b) Variation of the lattice parameter of $Zn(Se,S)_{x,100-x}$ as a function of the selenium fraction. (c) Raman spectrum of $InP/Zn(Se,S)_{50,50}$ core/shell QDs, synthesized using InP core QDs with a band-edge transition at 530 nm. The position of the relevant phonon lines of InP/ZnSe core/shell QDs with a similar InP core is indicated.

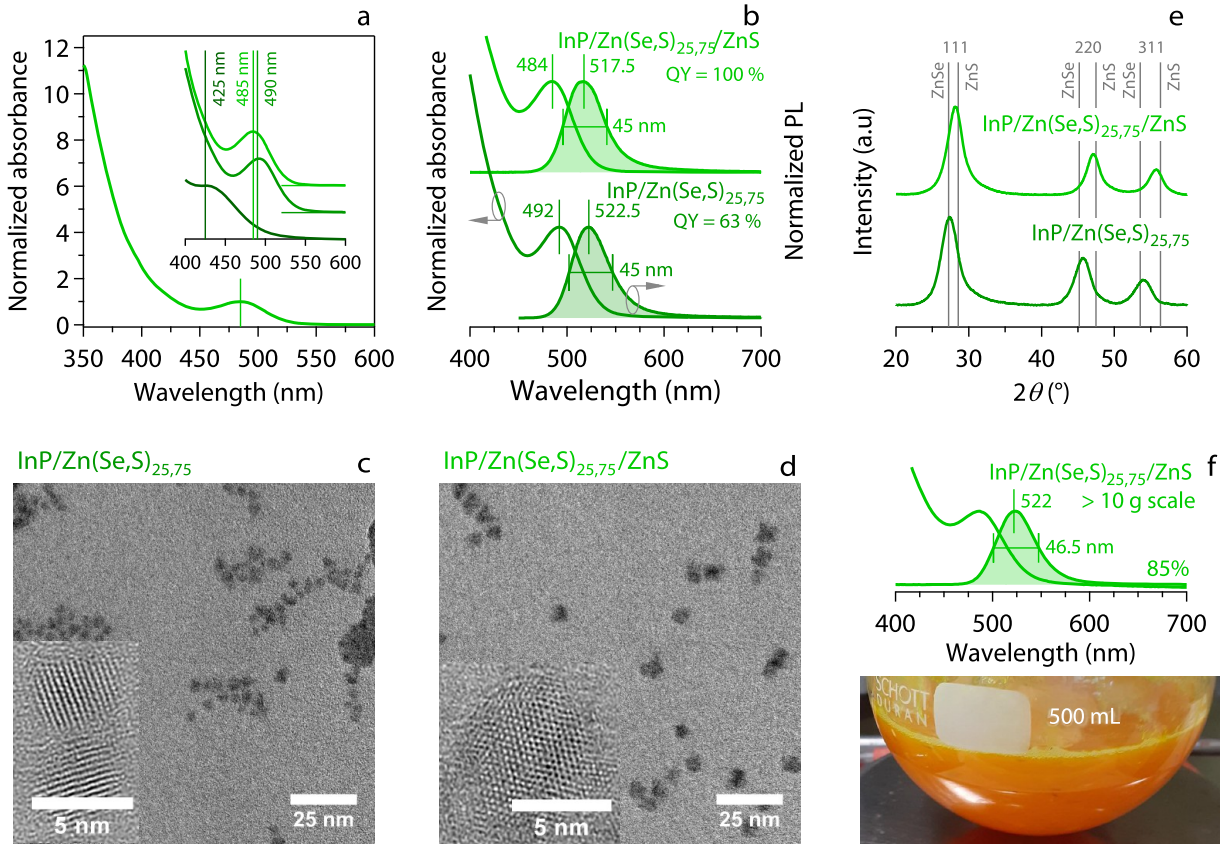

Figure 7. (a) Absorbance spectrum of $InP/Zn(Se,S)_{25,75}/ZnS$ core/shell/shell QDs. Inset: zoom of the absorbance spectrum of (dark green) InP core QDs, (medium green) $InP/Zn(Se,S)_{25,75}$ core/shell QDs, and (light green) $InP/Zn(Se,S)_{25,75}/ZnS$ core/shell/shell QDs. The maximum of the band-edge absorbance is indicated in all cases. (b) Absorbance and emission spectra of $InP/Zn(Se,S)_{25,75}$ core/shell and $InP/Zn(Se,S)_{25,75}/ZnS$ core/shell/shell QDs. The maximum emission wavelength, the line width, and the PLQY have been specified for each sample. (c, d) TEM and (inset) HRTEM micrographs of $InP/Zn(Se,S)_{25,75}$ core/shell and $InP/Zn(Se,S)_{25,75}/ZnS$ core/shell/shell QDs, showing a regular QD shape with respective average diameters of 4.4 ± 0.1 and 6.8 ± 0.1 nm with standard deviations of 0.7 and 1.1 nm. (e) X-ray diffraction patterns of $InP/Zn(Se,S)_{25,75}$ core/shell and $InP/Zn(Se,S)_{25,75}/ZnS$ core/shell/shell QDs. Vertical lines indicated the diffraction angles expected for ZnSe and ZnS as a reference. (f) Result of a +10 g synthesis of green-emitting $InP/Zn(Se,S)_{25,75}/ZnS$ core/shell/shell QDs, including (top) absorbance and photoluminescence spectra and (bottom) an image of the reaction flask.

observations agree with the occurrence of a minimal (3 nm) spectral blueshift and a minor (2−3 nm) broadening of the emission line.

Since the strain in the ZnSe shell in InP/ZnSe core/shell QDs is largely eliminated for thicker shells, we hypothesized that the best moment to add the ZnS outer shell occurs after a reaction time of 45−60 min for the precursor concentration and temperature profile used in the reference reaction. Thinner shells come with a more extended ZnSe lattice, which may compromise the formation of homogeneous ZnS shells. We

https://doi.org/10.1021/acsnano.2c03138
ACS Nano XXXX, XXX, XXX−XXX

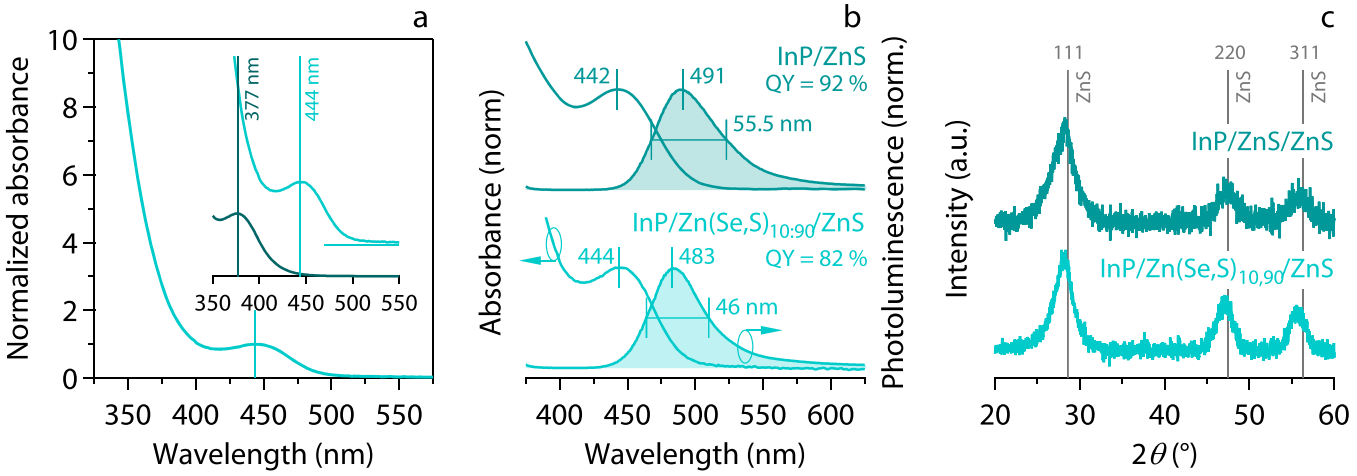

Figure 8. (a) Absorbance spectrum of InP/Zn(Se,S)$_{10,90}$/ZnS core/shell/shell QDs with a maximum band-edge absorbance at 444 nm. Inset. Zoom on the band-edge absorbance of (dark cyan) the initial InP core QDs and (cyan) the eventual InP/Zn(Se,S)$_{10,90}$/ZnS core/shell/shell QDs. (b) Absorbance and emission spectra of InP/Zn(Se,S)$_{10,90}$/ZnS core/shell/shell QDs. The maximum emission wavelength, the line width, and the PLQY have been specified. (c) X-ray diffraction patterns of InP/Zn(Se,S)$_{10,90}$/ZnS and InP/ZnS/ZnS core/shell/shell QDs nearly coincide with that of ZnS. Vertical lines indicate the diffraction angles expected for ZnS as a reference.

indeed observed more irregular ZnS shells in TEM micrographs of series 1 samples made using greater equivalent values of TOP-S; see the Supporting Information section S7. Thicker ZnSe shells, in contrast, extend the total reaction time while only attaining a marginal further narrowing of the emission line. Furthermore, in view of the reference reactions, the ZnS shell is best grown using 0.7 equiv of TOP-S, an amount that results in a shell thickness that yields a high PLQY while avoiding further line broadening. It was the synthesis protocol set up based on these considerations that was tested by three different collaborators and invariably yielded red-emitting InP/ZnSe/ZnS core/shell QDs with line widths between 45.5 and 47.5 nm and a PLQY of 90−95%; see Supporting Information section S5.

Full-Spectrum InP-Based QDs with Near-Unity Quantum Yield. As a next step, we investigated the extension of the proposed protocol to smaller InP cores so as to obtain amber-, green-, and cyan-emitting QDs. In this respect, the considerable redshift of the band-edge transition of the InP core QD forced us to adapt the ZnSe-ZnS shelling sequence applied to form red-emitting InP/ZnSe/ZnS QDs. As shown in Figure 6a, to end up with an emission line at around 520 nm, we needed InP core QDs with a band-edge transition in the range of 420−440 nm. Such wavelengths, however, correspond to an energy gap that is larger than the band gap of ZnSe. To enforce charge carrier confinement for such small InP core QDs, we therefore replaced the intermediate ZnSe shell by an alloyed Zn(Se,S)$_{x,100-x}$ shell, where x indicates the fraction of selenium. Since admixing sulfur will unavoidably increase the lattice mismatch with the InP core, we again evaluated the impact of an alloyed Zn(Se,S)$_{x,100-x}$ shell on the QD structure with Raman spectroscopy through the shift and the broadening of the InP phonon lines. Using a similar InP core QD as before, Figure 6b,c indicates that InP/Zn(Se,S)$_{50,50}$ core/shell QDs feature a further blueshift of the InP phonon band and a redshift of the ZnSe band as compared to InP/ZnSe, a variation in line with the expected reduction of the ZnSe lattice parameter upon sulfur admixing and the ensuing increase of the lattice mismatch with the InP core. Even so, the broadening of the InP phonon band is far less pronounced than found for plain ZnS shells; this result suggests that a switch to InP/Zn(Se,S)$_{x,100-x}$/ZnS core/shell QDs may better preserve the line width of the band-edge photoluminescence than a plain ZnS shell.

To form green-emitting InP-based QDs, we therefore first replaced $InCl_3$ and $ZnCl_2$ in the InP core synthesis by $InBr_3$ and $ZnBr_2$, in line with previous literature,[19] and used 7 equiv instead of 4 equiv of aminophosphine to form InP core QDs with a band-edge feature at around 430 nm; see Figure 7a. Next, these QDs were shelled by a Zn(Se,S)$_{25,75}$ alloy, grown by reacting zinc oleate with TOP-Se and TOP-S at 300 °C, added in a 1:3 ratio. As shown in Figure 7a, this shelling shifts the band-edge absorbance maximum to 490 nm and enhances the absorbance at wavelengths shorter than 380 nm. In this case, we applied interfacial treatment 1 prior to the shell growth. The resulting InP/Zn(Se,S)$_{25,75}$ exhibit a 45 nm wide band-edge photoluminescence band centered at 522.5 nm with a PLQY of 63%; see Figure 7b. Further completing the structure with a ZnS outer shell causes a slight blueshift in the emission line to 517.5 nm while preserving the line width and raising the PLQY to 100%. TEM imagesand X-ray diffraction patterns shown in Figure 7c−e and Supporting Information section S9 confirm that the synthesis proceeds as described. The diffraction features of the InP/Zn(Se,S)$_{25,75}$ core/shell QDs are shifted to slightly larger angles as compared to InP/ZnSe (see Figure 4d), and the resulting QDs, with an average diameter of 4.4 ± 0.1 nm with a standard deviation of 0.7 nm, are significantly larger than the initial InP core QDs. The final ZnS shell growth further shifts the diffraction pattern and results in somewhat larger overall QDs with sizes of 6.8 ± 0.1 nm and a standard deviation of 1.1 nm.

Upon extending the initial protocol for red-emitting InP-based QDs to form green-emitting InP-based QDs with near-unity PLQY, we observed that small details in the synthesis protocol impact the end result. Here, an interesting element is that the different reactivity of TOP-Se and TOP-S results in a changing shell composition with reaction time. As shown in Supporting Information section S9, a ZnSe-rich inner shell is grown in the initial stage of the shell growth reaction, while a gradual enrichment with ZnS follows in the later stage of the

https://doi.org/10.1021/acsnano.2c03138
ACS Nano XXXX, XXX, XXX−XXX

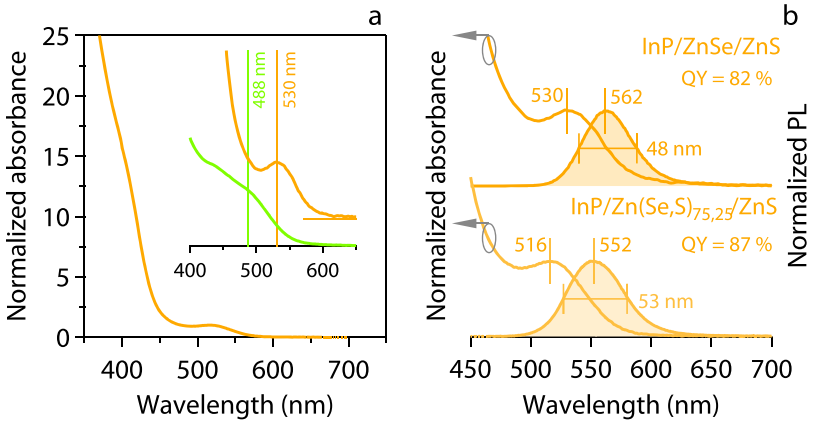

Figure 9. (a) Absorbance spectrum of InP/ZnSe/ZnS core/shell/shell QDs. Inset: zoom of the absorbance spectrum of (light green) InP core QDs, (amber) InP/ZnSe/ZnS core/shell/shell QDs. The maximum of the band-edge absorbance is indicated in all cases. (b) Absorbance and emission spectra of InP/ZnSe/ZnS and InP/$Zn(Se,S)_{75,25}$/ZnS core/shell/shell QDs as indicated. The maximum emission wavelength, the line width and the PLQY have been specified for each sample.

reaction. Such composition gradients can explain our finding that the heating rate after the start of the InP/$Zn(Se,S)_{25,75}$ shell affects the eventual line width of the photoluminescence; see Supporting Information section S9. As this impact of the heating rate on the line width was absent for red-emitting InP/ZnSe/ZnS QDs, we hypothesize that slower heating rates promote the initial growth of a selenium rich inner layer more than faster heating rates do. Such a ZnSe-rich inner shell can help mitigate strain induced by the core/shell lattice mismatch. This assumption agrees with recent literature, where near-unity green-emitting InP/Zn(Se,S)/ZnS and InP/ZnSe/ZnS QDs with line widths of 45 and 37 nm where reported, respectively,[12,14,15] even if the latter result was obtained by intermediate size fractionation of the InP core QDs. Furthermore, although 4 equiv of aminophosphine lead to QDs featuring a more pronounced band-edge absorbance, we found that a higher equivalent of aminophosphine led to a more narrow emission line and a higher PLQY after ZnS shell growth; see Supporting Information section S9. Finally, we tested the robustness of the established protocol by scaling up the reaction to form 10 g of green-emitting InP-based QDs. As shown in Figure 7f, the characteristics of the resulting QDs are nearly identical to those obtained at smaller scale.

In principle, the adaptations to the initial synthesis protocol we introduced for forming green-emitting InP-based QDs can be extended further to synthesize cyan-emitting InP-based QDs with a similar, near-unity PLQY. To explore that possibility, we replaced $InBr_3$ and $ZnBr_2$ with the corresponding iodides to form even smaller InP core QDs,[19] and we used a $Zn(Se,S)_{10,90}$ alloy as a shell to limit the spectral redshift by further promoting charge-carrier confinement in the InP core (see Figure 6a). As shown in Figure 8a, this approach results in core InP QDs with a maximum band-edge absorbance at 377 nm that shifts to 444 nm upon the sequential growth of a $Zn(Se,S)_{10,90}$ and a ZnS shell. Moreover, the final InP/$Zn(Se,S)_{10,90}$/ZnS core/shell/shell QDs feature a 46 nm wide emission line that has maximum intensity at 483 nm, i.e., at the edge of the cyan and blue spectral regions. In this case, we obtained a PLQY of 82%, a figure that we could enhance to +90% by using a plain ZnS shell, albeit at the expense of a line width increase to 55.5 nm; see Figure 8b. In line with the growth of a sulfur rich $Zn(Se,S)_{10,90}$ shell, the diffraction pattern of these cyan/blue emitting QDs nearly coincides with that of ZnS, see Figure 8c. So far, only few studies have reported the formation of cyan/blue InP-based QDs,[28,29,42,43] with highest PLQYs reported so far of 70% at a peak emission wavelength of 490 nm and a line width of 48 nm.[28]

Similarly, we explored adaptations to the initial red QD synthesis protocol to synthesize amber-emitting InP-based QDs. For that purpose, we replaced $ZnCl_2$ by $ZnBr_2$ to form slightly smaller InP core QDs,[19] and we tried either an intermediate shell formed from plain ZnSe or a $Zn(Se,S)_{75,25}$ alloy to analyze the balance between charge-carrier confinement in the InP core (see Figure 7a), and additional line broadening brought by an increased lattice mismatch. As shown in Figure 9a,b, this approach results in core InP QDs with a maximum band-edge absorbance at 488 nm, that shifts to 530 nm upon the sequential growth of a plain ZnSe and a ZnS shell. Moreover, the resulting InP/ZnSe/ZnS core/shell/shell QDs feature a 48 nm wide emission line that has maximum intensity at 562 nm. In this case, we obtained a PLQY of 82%, a figure that we could enhance to 87% by using a $Zn(Se,S)_{75,25}$ innershell, albeit at the expense of a line width increase to 53 nm (Figure 9b).

While the use of a $Zn(Se,S)_{75,25}$ alloyed shell reduces, as expected, the spectral redshift of the band-edge absorbance and emission of amber-emitting QDs, the increased line width reflects the delicate balance between promoting charge carrier confinement and inducing line broadening by changing the inner shell composition and increasing core/shell lattice mismatch. This point is further highlighted by the summary of the characteristics of the different InP-based QDs presented in Figures 2 and 7–9 and in Table 2. Moving from red- to

Table 2. Overview of Synthetic and Optical Characteristics of the Different InP-Based QDs Presented in This Work Organized According to Emission Color

color	shell composition	PL peak (nm)	fwhm (nm)	PLQY
red	ZnSe	607	45.5	95%
amber 1	ZnSe	562	48	82%
amber 2	$Zn(Se,S)_{75,25}$	552	53	87%
green	$Zn(Se,S)_{25,75}$	517.5	45	100%
cyan 1	$Zn(Se,S)_{10,90}$	483	46	82%
cyan 2	ZnS	491	55.5	92%

https://doi.org/10.1021/acsnano.2c03138
ACS Nano XXXX, XXX, XXX−XXX

cyan-emitting QDs, one sees that for a given emission wavelength, an increased sulfur content in the inner shell raises the PLQY at the expense of the emission line width. However, a larger lattice mismatch has less impact on the emission line width of smaller InP core QDs, a finding probably reflecting the larger tolerance of smaller core QDs for core/shell lattice mismatch.[44,45] The resulting possibility to gradually increase the sulfur content of inner shell with decreasing InP core size is what enables InP-based QDs with narrow emission lines and a near unity PLQY to be formed across the full visible spectrum.

CONCLUSION

We developed a highly reproducible approach to synthesize colloidal InP/Zn(Se,S)$_{x,100-x}$/ZnS core/shell/shell QDs. Rational adaptations of a common synthesis protocol to change the core size and adjust the intermediate shell composition enable a full tuning across the visible spectrum from cyan/blue to red. Moreover, the passivation of the intermediate Zn(Se,S)$_{x,100-x}$ shell by a ZnS outer shell results in a near-unity photoluminescence efficiency across this entire spectral window, and careful control of the strain induced by the shell growth keeps the emission line width close to 45 nm, regardless of the emission wavelength. The possibility to form such high-quality QDs with variable emission wavelengths will strongly promote research into the optoelectronic properties of InP-based QDs. Moreover, in view of luminescent color conversion, the combination of spectral tunability and near-unity PLQY enables efficiency losses and heating due to self-absorption to be suppressed in applications ranging from solar concentrators to high color-rendering white LEDs and micro-LED displays. Even so, further improvements to the proposed synthesis method are needed, in particular to make the emission more narrow and symmetrical and shift the central emission line deeper in the blue part of the visible spectrum to enable, for example, full conversion of near-UV light in visible spectra-on-demand.

METHODS

Quantum Dot Synthesis. Collodial InP/ZnSe/ZnS were synthesized through adaptations of a previously published method,[19] which will be detailed here for the case of red-emitting QDs. An exhaustive description of the precursor preparation and all synthesis protocols can be found in Supporting Information section S2. To start the synthesis, 100 mg (0.45 mmol) of indium(III) chloride as indium raw material and 300 mg (2.20 mmol) of zinc(II) chloride as zinc raw material were mixed in 3 mL (9.10 mmol) of anhydrous oleylamine. The mixture was stirred and degassed at 120 °C for an hour and then heated to 180 °C under inert atmosphere. Upon reaching 180 °C, 0.50 mL (1.83 mmol) of tris(diethylamino)phosphine, transaminated with 2 mL (6.07 mmol) of anhydrous oleylamine, was quickly injected in the reaction mixture described above and the InP nanocrystal synthesis proceeded. After 30 min, the dispersion was cooled to 120 °C, and 120 mg (0.31 mmol) of tetrabutylammonium hexafluorophosphate, 0.3 mL (16.65 mmol) of water, and 2 g (3.18 mmol) of zinc(II) oleate mixed in 2 mL (6.07 mmol) of oleylamine and 4 mL (12.50 mmol) of 1-octadecene were added as a surface treatment prior to ZnSe shell growth. Subsequently, the mixture was stirred and degassed for an hour. Afterward, 1.6 mL of a stoichiometric TOP-Se (2.24 M) solution was injected, and the temperature was raised to 330 °C. At this temperature, the shell growth went on for 28−60 min. Subsequent to the ZnSe shell growth, the reaction mixture was cooled down to 120 °C, after which 400 mg (2.21 mmol) of zinc(II)acetate was added and the mixture was stirred and degassed for 1 h. Consecutively, 1 mL of a stoichiometric TOP-S (2.24 M) solution was injected, and the temperature was raised to 300 °C. After 1 h of ZnS shell growth, the temperature had been set to 240 °C and 1 mL (4.18 mmol) of dodecanethiol was injected. Ten minutes later, the reaction was stopped by cooling down the mixture to room temperature. InP/ZnSe/ZnS QDs were then precipitated once using acetone, redispersed in toluene, and stored in a N_2-filled glovebox.

Material Characterization. UV−vis spectra were recorded on a PerkinElmer Lambda 365 UV−vis spectrophotometer. XRD analysis was conducted on a Thermo Scientific ARL X'Tra diffractometer, operated at 40 kV/30 mA using Cu Kα radiation (λ = 1.5406 Å) and a Peltier cooled Si(Li) solid-state dectector. Energy-dispersive X-ray spectroscopy (EDS) was carried out with a JEOL EX 24065 JGP. Transmission electron microscopy (TEM) images were recorded on a JEOL JEM-2200FS transmission electron microscope at 200 kV with the QDs deposited on copper grids coated with ultrathin carbon film. PL spectra were taken on a Edinburgh Instruments FLSP920 spectrophotometer. The absolute PLQY was measured using an integrating sphere. For Raman spectroscopy, the QD solutions were drop-cast on gold foil. As an excitation source, a solid-state laser (Cobolt) with 437 nm wavelength was chosen; the laser spot was focused to approximately 1 μm in diameter on the sample and laser power was held around 0.1 mW for all measurements to prevent damage or heating of the samples. Raman spectra were recorded under ambient conditions in backscattering geometry using a Horiba T64000 spectrometer equipped with a 1800 gr/mm grating and a nitrogen-cooled CCD for spectrum acquisition. For each sample, multiple spectra were acquired from several sample spots. There were no significant differences in the spectra and no degradation visible within one set of measurements of the same sample. Each set of spectra was calibrated using neon lines.

ASSOCIATED CONTENT

Supporting Information

The Supporting Information is available free of charge at https://pubs.acs.org/doi/10.1021/acsnano.2c03138.

Assessment of the impact of self-absorption on the external quantum efficiency, detailed description of experimental procedures, analysis of interfacial oxidation, impact of zinc acetate addition, protocol reproducibility evaluation, full characterization of the In-based benchmark QDs, full characterization of the series 1 InP/ZnS/ZnS QDs, full characterization of the series 2 InP/ZnSe QDs, and details on the formation and characteristics of green-emitting InP QDs (PDF)

AUTHOR INFORMATION

Corresponding Author

Zeger Hens − *Physics and Chemistry of Nanostructures and Center for Nano and Biophotonics, Ghent University, Gent 9000, Belgium;* orcid.org/0000-0002-7041-3375; Email: zeger.hens@ugent.be

Authors

Hannes Van Avermaet − *Physics and Chemistry of Nanostructures and Center for Nano and Biophotonics, Ghent University, Gent 9000, Belgium*

Pieter Schiettecatte − *Physics and Chemistry of Nanostructures and Center for Nano and Biophotonics, Ghent University, Gent 9000, Belgium;* orcid.org/0000-0002-0178-413X

Sandra Hinz − *Institute of Physical Chemistry, Universität Hamburg, Hamburg 20146, Germany; Institute of Condensed Matter Physics, Friedrich-Alexander-Universität Erlangen-Nürnberg, Erlangen 91058, Germany*

https://doi.org/10.1021/acsnano.2c03138
ACS Nano XXXX, XXX, XXX−XXX

Luca Giordano − *Physics and Chemistry of Nanostructures and Center for Nano and Biophotonics, Ghent University, Gent 9000, Belgium*
Fabio Ferrari − *Laboratoire de Physique et Chimie des Nano-Objets, Université de Toulouse, CNRS, INSA, UPS, Toulouse CEDEX-4 31077, France*
Céline Nayral − *Laboratoire de Physique et Chimie des Nano-Objets, Université de Toulouse, CNRS, INSA, UPS, Toulouse CEDEX-4 31077, France*
Fabien Delpech − *Laboratoire de Physique et Chimie des Nano-Objets, Université de Toulouse, CNRS, INSA, UPS, Toulouse CEDEX-4 31077, France;* orcid.org/0000-0003-1517-1331
Janina Maultzsch − *Institute of Condensed Matter Physics, Friedrich-Alexander-Universität Erlangen-Nürnberg, Erlangen 91058, Germany*
Holger Lange − *Institute of Physical Chemistry, Universität Hamburg, Hamburg 20146, Germany;* orcid.org/0000-0002-4236-2806
Complete contact information is available at: https://pubs.acs.org/10.1021/acsnano.2c03138

Notes

The authors declare no competing financial interest.

ACKNOWLEDGMENTS

Z.H. and H.V.A acknowledge SIM-Flanders (SBO QDOCCO, ICON QUALIDI) for research funding. Z.H. acknowledges the FWO-Vlaanderen (research project G0B2921N) and Ghent University (BOF-GOA 01G01019) for research funding. P.S. acknowledges the Agentschap Innoveren en Ondernemen (VLAIO, REQLED2020) for research funding. S.H., J.M., and H.L. acknowledge support by the Deutsche Forschungsgemeinschaft (DFG) under grant numbers EXC 2056, project ID 390715994, LA 2901/5-1, and MA 4079/14-1.

REFERENCES

(1) Reiss, P.; Protière, M.; Li, L. Core/Shell Semiconductor Nanocrystals. *Small* **2009**, *5*, 154−168.
(2) Kim, T. H.; Jun, S.; Cho, K. S.; Choi, B. L.; Jang, E. Bright and Stable Quantum Dots and Their Applications in Full-Color Displays. *MRS Bull.* **2013**, *38*, 712−720.
(3) Kovalenko, M. V.; Manna, L.; Cabot, A.; Hens, Z.; Talapin, D. V.; Kagan, C. R.; Klimov, X. V. I.; Rogach, A. L.; Reiss, P.; Milliron, D. J.; et al. Prospects of Nanoscience with Nanocrystals. *ACS Nano* **2015**, *9*, 1012−1057.
(4) Steckel, J. S.; Ho, J.; Hamilton, C.; Xi, J.; Breen, C.; Liu, W.; Allen, P.; Coe-Sullivan, S. Quantum Dots: The Ultimate Down-Conversion Material for LCD Displays. *J. Soc. Inf. Display* **2015**, *23*, 294−305.
(5) Shimizu, K. T.; Böhmer, M.; Estrada, D.; Gangwal, S.; Grabowski, S.; Bechtel, H.; Kang, E.; Vampola, K. J.; Chamberlin, D.; Shchekin, O. B.; et al. Toward Commercial Realization of Quantum Dot Based White Light-Emitting Diodes for General Illumination. *Photon. Res.* **2017**, *5*, A1−A6.
(6) Meinardi, F.; Colombo, A.; Velizhanin, K. A.; Simonutti, R.; Lorenzon, M.; Beverina, L.; Viswanatha, R.; Klimov, V. I.; Brovelli, S. Large-Area Luminescent Solar Concentrators Based on 'Stokes-Shift-Engineered' Nanocrystals in a Mass-Polymerized PMMA Matrix. *Nat. Photonics* **2014**, *8*, 392−399.
(7) Yang, J.; Choi, M. K.; Yang, U. J.; Kim, S. Y.; Kim, Y. S.; Kim, J. H.; Kim, D. H.; Hyeon, T. Toward Full-Color Electroluminescent Quantum Dot Displays. *Nano Lett.* **2021**, *21*, 26−33.
(8) Won, Y. H.; Cho, O.; Kim, T.; Chung, D. Y.; Kim, T.; Chung, H.; Jang, H.; Lee, J.; Kim, D.; Jang, E. Highly Efficient and Stable InP/ZnSe/ZnS Quantum Dot Light-Emitting Diodes. *Nature* **2019**, *575*, 634−638.
(9) Karadza, B.; Van Avermaet, H.; Mingabudinova, L.; Hens, Z.; Meuret, Y. Efficient, High-CRI White LEDs by Combining Traditional Phosphors with Cadmium-Free InP/ZnSe Red Quantum Dots. *Photon. Res.* **2022**, *10*, 155−165.
(10) Hines, M. A.; Guyot-Sionnest, P. Synthesis and Characterization of Strongly Luminescing ZnS-Capped CdSe Nanocrystals. *J. Phys. Chem.* **1996**, *100*, 468−471.
(11) Chen, O.; Zhao, J.; Chauhan, V. P.; Cui, J.; Wong, C.; Harris, D. K.; Wei, H.; Han, H.-S.; Fukumura, D.; Jain, R. K.; et al. Compact High-Quality CdSe-CdS Core-Shell Nanocrystals with Narrow Emission Linewidths and Suppressed Blinking. *Nat. Mater.* **2013**, *12*, 445−451.
(12) Kim, Y.; Ham, S.; Jang, H.; Min, J. H.; Chung, H.; Lee, J.; Kim, D.; Jang, E. Bright and Uniform Green Light Emitting InP/ZnSe/ZnS Quantum Dots for Wide Color Gamut Displays. *ACS Appl. Nano Mater.* **2019**, *2*, 1496−1504.
(13) Li, Y.; Hou, X.; Dai, X.; Yao, Z.; Lv, L.; Jin, Y.; Peng, X. Stoichiometry-Controlled InP-Based Quantum Dots: Synthesis, Photoluminescence, and Electroluminescence. *J. Am. Chem. Soc.* **2019**, *141*, 6448−6452.
(14) Liu, P.; Lou, Y.; Ding, S.; Zhang, W.; Wu, Z.; Yang, H.; Xu, B.; Wang, K.; Sun, X. W. Green InP/ZnSeS/ZnS Core Multi-Shelled Quantum Dots Synthesized with Aminophosphine for Effective Display Applications. *Adv. Funct. Mater.* **2021**, *31*, 2008453.
(15) Jo, J. H.; Jo, D. Y.; Choi, S. W.; Lee, S. H.; Kim, H. M.; Yoon, S. Y.; Kim, Y.; Han, J. N.; Yang, H. Highly Bright, Narrow Emissivity of InP Quantum Dots Synthesized by Aminophosphine: Effects of Double Shelling Scheme and Ga Treatment. *Adv. Opt. Mater.* **2021**, *9*, 2100427.
(16) Chae, H.; Jiang, W. Efficiency Enhancement of Tris-(dimethylamino)-Phosphine-Based Red Indium Phosphide Quantum-Dot Light-Emitting Diodes via Chlorine-Doped ZnMgO Electron Transport Layers. *J. Phys. Chem. C* **2020**, *124*, 25221−25228.
(17) Choi, S. W.; Kim, H. M.; Yoon, S. Y.; Jo, D. Y.; Kim, S. K.; Kim, Y.; Park, S. M.; Lee, Y. J.; Yang, H. Aminophosphine-Derived, High-Quality Red-Emissive InP Quantum Dots by the Use of an Unconventional In Halide. *J. Mater. Chem. C* **2022**, *10*, 2213−2222.
(18) Yu, P.; Shan, Y.; Cao, S.; Hu, Y.; Li, Q.; Zeng, R.; Zou, B.; Wang, Y.; Zhao, J. Inorganic Solid Phosphorus Precursor of Sodium Phosphaethynolate for Synthesis of Highly Luminescent InP-Based Quantum Dots. *ACS Energy Lett.* **2021**, *6*, 2697−2703.
(19) Tessier, M. D.; Dupont, D.; De Nolf, K.; De Roo, J.; Hens, Z. Economic and Size-Tunable Synthesis of InP/ZnE (E = S, Se) Colloidal Quantum Dots. *Chem. Mater.* **2015**, *27*, 4893−4898.
(20) Jeong, B. G.; Chang, J. H.; Hahm, D.; Rhee, S.; Park, M.; Lee, S.; Kim, Y.; Shin, D.; Park, J. W.; Lee, C.; et al. Interface Polarization in Heterovalent Core−Shell Nanocrystals. *Nat. Mater.* **2021**, *29*, 246−252.
(21) Park, N.; Eagle, F. W.; DeLarme, A. J.; Monahan, M.; LoCurto, T.; Beck, R.; Li, X.; Cossairt, B. M. Tuning the Interfacial Stoichiometry of InP core and InP/ZnSe Core/Shell Quantum Dots. *J. Chem. Phys.* **2021**, *155*, 084701.
(22) Tessier, M. D.; Baquero, E. A.; Dupont, D.; Grigel, V.; Bladt, E.; Bals, S.; Coppel, Y.; Hens, Z.; Nayral, C.; Delpech, F. Interfacial Oxidation and Photoluminescence of InP-Based Core/Shell Quantum Dots. *Chem. Mater.* **2018**, *30*, 6877−6883.
(23) Vikram, A.; Zahid, A.; Bhargava, S. S.; Jang, H.; Sutrisno, A.; Khare, A.; Trefonas, P.; Shim, M.; Kenis, P. J. Unraveling the Origin of Interfacial Oxidation of InP-Based Quantum Dots: Implications for Bioimaging and Optoelectronics. *ACS Applied Nano Materials* **2020**, *3*, 12325−12333.
(24) Tessier, M. D.; De Nolf, K.; Dupont, D.; Sinnaeve, D.; De Roo, J.; Hens, Z. Aminophosphines: A Double Role in the Synthesis of Colloidal Indium Phosphide Quantum Dots. *J. Am. Chem. Soc.* **2016**, *138*, 5923−5929.

(25) Cros-Gagneux, A.; Delpech, F.; Nayral, C.; Cornejo, A.; Coppel, Y.; Chaudret, B. Surface Chemistry of InP Quantum Dots: A Comprehensive Study. *J. Am. Chem. Soc.* **2010**, *132*, 18147−18157.
(26) Wang, H. C.; Zhang, H.; Chen, H. Y.; Yeh, H. C.; Tseng, M. R.; Chung, R. J.; Chen, S.; Liu, R. S. Cadmium-Free InP/ZnSeS/ZnS Heterostructure-Based Quantum Dot Light-Emitting Diodes with a ZnMgO Electron Transport Layer and a Brightness of Over 10 000 cd/m2. *Small* **2017**, *13*, 1603962.
(27) Ramasamy, P.; Kim, N.; Kang, Y. S.; Ramirez, O.; Lee, J. S. Tunable, Bright, and Narrow-Band Luminescence from Colloidal Indium Phosphide Quantum Dots. *Chem. Mater.* **2017**, *29*, 6893−6899.
(28) Kim, K. H.; Jo, J. H.; Jo, D. Y.; Han, C. Y.; Yoon, S. Y.; Kim, Y.; Kim, Y. H.; Ko, Y. H.; Kim, S. W.; Lee, C.; et al. Cation-Exchange-Derived InGaP Alloy Quantum Dots toward Blue Emissivity. *Chem. Mater.* **2020**, *32*, 3537−3544.
(29) Zhang, W.; Ding, S.; Zhuang, W.; Wu, D.; Liu, P.; Qu, X.; Liu, H.; Yang, H.; Wu, Z.; Wang, K.; et al. InP/ZnS/ZnS Core/Shell Blue Quantum Dots for Efficient Light-Emitting Diodes. *Adv. Funct. Mater.* **2020**, *30*, 2005303.
(30) Ryu, E.; Kim, S.; Jang, E.; Jun, S.; Jang, H.; Kim, B.; Kim, S.-w. Step-Wise Synthesis of InP/ZnS Core-Shell Quantum Dtos and the Role of Zinc Acetate. *Chem. Mater.* **2009**, *21*, 573−575.
(31) Banski, M.; Chrzanowski, M.; Zatryb, G.; Misiewicz, J.; Podhorodecki, A. Enhanced Photoluminescence Stability of CdS Nanocrystals Through a Zinc Acetate Reagent. *RSC Adv.* **2018**, *8*, 25417−25422.
(32) Pietra, F.; De Trizio, L.; Hoekstra, A. W.; Renaud, N.; Prato, M.; Grozema, F. C.; Baesjou, P. J.; Koole, R.; Manna, L.; Houtepen, A. J. Tuning the Lattice Parameter of InxZnyP for Highly Luminescent Lattice-Matched Core/Shell Quantum Dots. *ACS Nano* **2016**, *10*, 4754−4762.
(33) Pietra, F.; Kirkwood, N.; De Trizio, L.; Hoekstra, A. W.; Kleibergen, L.; Renaud, N.; Koole, R.; Baesjou, P.; Manna, L.; Houtepen, A. J. Ga for Zn Cation Exchange Allows for Highly Luminescent and Photostable InZnP-Based Quantum Dots. *Chem. Mater.* **2017**, *29*, 5192−5199.
(34) Rafipoor, M.; Dupont, D.; Tornatzky, H.; Tessier, M. D.; Maultzsch, J.; Hens, Z.; Lange, H. Strain Engineering in InP/(Zn,Cd)Se Core/Shell Quantum Dots. *Chem. Mater.* **2018**, *30*, 4393−4400.
(35) Rafipoor, M.; Tornatzky, H.; Dupont, D.; Maultzsch, J.; Tessier, M. D.; Hens, Z.; Lange, H. Strain in InP/ZnSe, S Core/Shell Quantum Dots From Lattice Mismatch and Shell Thickness - Material Stiffness Influence. *J. Chem. Phys.* **2019**, *151*, 154704.
(36) Cavanaugh, P.; Jen-La Plante, I.; Ippen, C.; Ma, R.; Kelley, D. F.; Kelley, A. M. Resonance Raman Study of Shell Morphology in InP/ZnSe/ZnS Core/Shell/Shell Nanocrystals. *J. Phys. Chem. C* **2021**, *125*, 10549−10557.
(37) Abstreiter, G.; Cardona, M.; Pinczuk, A. Light scattering by free carrier excitations in semiconductors. *Top. Appl. Phys.* **1984**, *54*, 5−150.
(38) Scamarcio, G.; Lugará, M.; Manno, D. Size-Dependent Lattice Contraction in $CdS_{1-x}Se_x$ Nanocrystals Embedded in Glass Observed by Raman Scattering. *Phys. Rev. B* **1992**, *45*, 13792−13795.
(39) Trommer, R.; Müller, H.; Cardona, M.; Vogl, P. Dependence of the Phonon Spectrum of InP on Hydrostatic Pressure. *Phys. Rev. B* **1980**, *21*, 4869−4878.
(40) Boldt, K. Raman Spectroscopy of Colloidal Semiconductor Nanocrystals. *Nano Futures* **2022**, *6*, 012003.
(41) Lange, H.; Kelley, D. F. Spectroscopic Effects of Lattice Strain in InP/ZnSe and InP/ZnS Nanocrystals. *J. Phys. Chem. C* **2020**, *124*, 22839−22844.
(42) Park, J. P.; Lee, J. J.; Kim, S. W. Highly Luminescent InP/GaP/ZnS QDs Emitting in the Entire Color Range via a Heating Up Process. *Sci. Rep.* **2016**, *6*, 30094.
(43) Lee, W.; Lee, C.; Kim, B.; Choi, Y.; Chae, H. Synthesis of Blue-Emissive InP/GaP/ZnS Quantum Dots via Controlling the Reaction Kinetics of Shell Growth and Length of Capping Ligands. *Nanomaterials* **2020**, *10*, 2171.
(44) Smith, A. M.; Mohs, A. M.; Nie, S. Tuning the Optical and Electronic Properties of Colloidal Nanocrystals by Lattice Strain. *Nat. Nanotechnol.* **2009**, *4*, 56−63.
(45) Gong, K.; Kelley, D. F. Lattice Strain Limit for Uniform Shell Deposition in Zincblende CdSe/CdS Quantum Dots. *J. Phys. Chem. Lett.* **2015**, *6*, 1559−1562.

https://doi.org/10.1021/acsnano.2c03138
ACS Nano XXXX, XXX, XXX−XXX